Reconstituted Fusion Pore

Aleksandar Jeremic,* Marie Kelly,* Sang-Joon Cho,* Marvin H. Stromer,† and Bhanu P. Jena*
*Department of Physiology, Wayne State University School of Medicine, Detroit, Michigan 48201; and †Department of Animal Science, Biochemistry, Biophysics, and Molecular Biology, Iowa State University, Ames, Iowa 50011

ABSTRACT Fusion pores or porosomes are basket-like structures at the cell plasma membrane, at the base of which, membrane-bound secretory vesicles dock and fuse to release vesicular contents. Earlier studies using atomic force microscopy (AFM) demonstrated the presence of fusion pores at the cell plasma membrane in a number of live secretory cells, revealing their morphology and dynamics at nm resolution and in real time. ImmunoAFM studies demonstrated the release of vesicular contents through the pores. Transmission electron microscopy (TEM) further confirmed the presence of fusion pores, and immunoAFM, and immunochemical studies demonstrated t-SNAREs to localize at the base of the fusion pore. In the present study, the morphology, function, and composition of the immunoisolated fusion pore was investigated. TEM studies reveal in further detail the structure of the fusion pore. Immunoblot analysis of the immunoisolated fusion pore reveals the presence of several isoforms of the proteins, identified earlier in addition to the association of chloride channels. TEM and AFM micrographs of the immunoisolated fusion pore complex were superimposable, revealing its detail structure. Fusion pore reconstituted into liposomes and examined by TEM, revealed a cup-shaped basket-like morphology, and were functional, as demonstrated by their ability to fuse with isolated secretory vesicles.

INTRODUCTION

Essential physiological processes such as neurotransmission, and the secretion of enzymes or hormones, require fusion of membrane-bound secretory vesicles at the cell plasma membrane (PM) and the consequent expulsion of vesicular contents. Using atomic force microscopy (AFM), the existence of the fusion pore was demonstrated, and its structure and dynamics in both exocrine (Schneider et al., 1997; Cho et al., 2002c,d) and neuroendocrine cells (Cho et al., 2002a,b) examined, at near nm resolution and in real time. Fusion pores in NG108-15 nerve cells have also been reported (Tojima et al., 2000). Electron microscopy later confirmed the presence of the fusion pore and revealed its morphology in greater detail (Jena et al., 2003). The composition of the fusion pore or porosome has also been revealed from these recent studies (Jena et al., 2003).

Live pancreatic acinar cells in physiological buffer when imaged by AFM, reveal at the apical PM where secretion is known to occur, a group of circular ''pits'' measuring 0.4–1.2 μm in diameter, containing smaller ''depressions'' within (Cho et al., 2002c; Schneider et al., 1997), (Figs. 1 and 2). On average, there are three to four depressions within a pit, each depression measuring between 100 and 150 nm in diameter. The basolateral membrane of acinar cells are devoid of either pits or depressions. High resolution AFM images of depressions in live cells further reveal a cone-shaped morphology (Fig. 1, *c* and *d*). Similar to acinar cells of the exocrine pancreas, neuroendocrine cells such as the growth hormone (GH) secreting cells of the pituitary gland and chromaffin cells, possess both pits and depressions in their PM (Cho et al., 2002a,b). When pancreatic acinar cells were exposed to a secretory stimulus, a time-dependent increase in depression diameter (20–35%), followed by a return to resting size after completion of secretion was observed (Cho et al., 2002a,c; Schneider et al., 1997). No demonstrable change, however, in pit size was detected during this time (Schneider et al., 1997). Enlargement of depression diameter and an increase in its relative depth after exposure to a secretory stimulus, correlated with increased secretion. Conversely, exposure of pancreatic acinar cells to cytochalasin B, a fungal toxin that inhibits actin polymerization, resulted in a 15–20% decrease in depression size, and a consequent 50–60% loss in stimulated secretion. These studies suggested depressions to be the fusion pores in pancreatic acinar cells, where secretory vesicles dock and fuse to release vesicular contents. These studies further demonstrated the involvement of actin in regulation of the structure and function of depressions. As eluded earlier resting GH secreting cells of the pituitary gland (Cho et al., 2002a) and chromaffin cells of the adrenal medulla (Cho et al., 2002b), both revealed the presence of pits and depressions at the cell PM. Depressions in resting GH cells measured 154 $\pm$ 4.5 nm (mean $\pm$ SE) in diameter, demonstrating a 40% increase (215 $\pm$ 4.6 nm; $p < 0.01$) after stimulation of secretion. Once again, similar to acinar cells, no appreciable change in pit size was demonstrated in the neuroendocrine cells after stimulation of secretion. Decrease in depression size and the loss in ability to secrete, after exposure to an actin depolymerizing agent (Schneider et al., 1997), suggested depressions to be the fusion pores. A direct demonstration that depressions are fusion pores, came later from immunoAFM studies (Cho et al., 2002a,c). After

Submitted May 19, 2003, and accepted for publication June 27, 2003.

Aleksandar Jeremic and Marie Kelly contributed equally to this work.

Address reprint requests to Bhanu P. Jena, Ph.D., Dept. of Physiology, Wayne State University School of Medicine, 5239 Scott Hall, 540 E. Canfield Ave., Detroit, MI 48201-4177. Tel.: 313-577-1532; Fax: 313-993-4177; E-mail: bjena@med.wayne.edu.

0006-3495/03/09/2035/09 $2.00

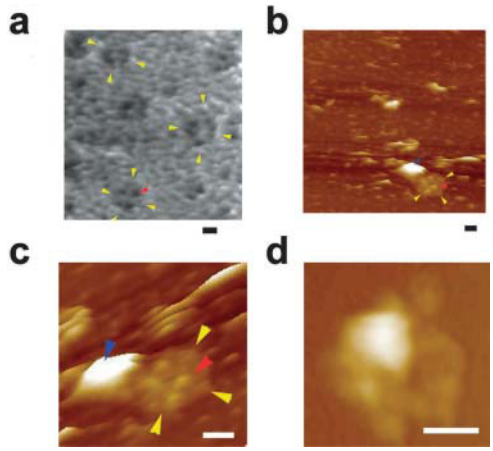

FIGURE 1 AFM micrographs of fusion pores at the surface of apical plasma membrane in live pancreatic acinar cells and at the cytosolic side of isolated pancreatic plasma membrane preparations. (*a*) Several circular ''pits'' (*yellow arrowheads*) with fusion pores (*red arrowheads*) are seen in this AFM micrograph of the apical plasma membrane in live pancreatic acinar cell. (*b*) AFM micrograph of the cytosolic side of isolated pancreatic plasma membrane preparation depicting a ''pit'' (*yellow arrowheads*) containing several inverted cup-shaped fusion pores (*red arrowhead*) within, associated with a ZG (*blue arrowhead*). (*c*) The ''pit'' and inverted fusion pores in *b* is shown at higher magnification. (*d*) AFM micrograph of another ''pit'' with inverted fusion pores within, and associated with a ZG, is shown. Bar = 200 nm.

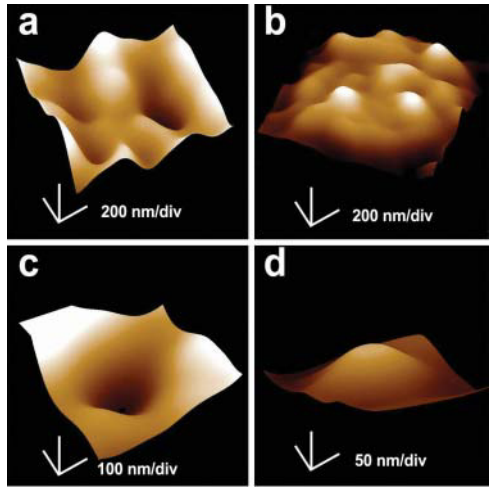

FIGURE 2 AFM micrographs of the fusion pore or porosome, as it appears at the cell surface and at the cytosolic side. (*a*) A pit with four fusion pores within, found at the apical surface in a live pancreatic acinar cell. (*b*) AFM micrograph of isolated plasma membrane preparation reveals the cytosolic end of a pit with inverted cup-shaped structures, the fusion pores. (*c*) A single fusion pore at the cell surface, and (*d*) as it appears at the cytosolic side of the cell membrane.

stimulation of secretion, the specific localization of secretory protein at depressions, confirmed depressions to be the fusion pores.

The morphology of the fusion pore at the cytosolic side of the cell was next revealed using AFM and immunoAFM studies on isolated PM preparations (Jena et al., 2003). Scattered circular disks or pits, measuring 0.5–1 μm in diameter, with 15–25 nm in height inverted cup-shaped fusion pores (Fig. 1, *b* and *d*), were observed. Conformation that the inverted cups are fusion pores, as they appear from within the cell, was revealed from AFM studies demonstrating attached secretory vesicles, and from immunoAFM studies demonstrating the localization of t-SNARE proteins at the base of the fusion pore or porosome cup (Jena et al., 2003). Target membrane proteins, SNAP-25 and syntaxin (t-SNARE) and secretory vesicle associated membrane protein (v-SNARE), are part of the conserved protein complex involved in fusion of opposing bilayers (Rothman, 1994; Weber et al., 1998). Because membrane-bounded secretory vesicles dock and fuse at depressions to release vesicular contents, it was suggested that PM-associated t-SNAREs are part of the fusion pore complex. It was no surprise therefore, that the t-SNARE protein SNAP-23, implicated in secretion from pancreatic acinar cells (Gaisano et al., 1997), was located at the tip of the inverted cup where secretory vesicles would dock and fuse. The structure of the fusion pore was further determined using transmission electron microscopy (TEM) (Jena et al., 2003). TEM studies confirm the fusion pore to have a cup-shaped structure, with similar dimensions as determined in all our AFM studies (Cho et al., 2002a,b,c,d; Schneider et al., 1997). Additionally, TEM results reveal that the fusion pore, has a basket-like morphology, with three lateral and a number of vertically arranged ridges, and a ring at the base of the fusion pore cup (Jena et al., 2003). Because fusion pores or porosomes are stable structures at the cell PM, we hypothesized that if membrane-bounded secretory vesicles or zymogen granules (ZGs) were to fuse at the base of the fusion pore, it should be possible to isolate ZG-associated fusion pore complexes. Indeed, TEM of isolated ZG preparations revealed the presence of fusion pore associated with docked vesicle (Jena et al., 2003). As observed in whole cells, vertical structures originate from within the fusion pore complex and appear attached to the fusion pore membrane. The presence of vertical ridges lining the fusion pore, have also been reported in NG108-15 nerve cells (Tojima, et al., 2000).

In an earlier study using SNARE proteins and artificial lipid membranes, we demonstrated that t- and v-SNAREs located in opposing bilayers, interact in a circular array to form conducting pores (Cho et al., 2002e). Because similar 45–50 nm circular structures were observed at the base of the fusion pore, and SNAP-23 immunoreactivity was found to localize at this site, the presence of t-SNAREs at the base of the fusion pore cup was further demonstrated (Cho et al., 2002e). In the last decade, a number of studies demonstrate the involvement of cytoskeletal proteins in exocytosis, and some studies implicate direct interaction of cytoskeleton protein with SNAREs (Bennett, 1990; Cho et al., 2002c; Faigle et al., 2000; Goodson et al., 1997; Nakano et al., 2001; Ohyama et al., 2001). Furthermore, actin and microtubule-based cytoskeleton has been implicated in intracellular

vesicle traffic (Goodson et al., 1997). Fodrin, which was previously implicated in exocytosis (Bennett, 1990), has recently been shown to directly interact with SNAREs (Nakano et al., 2001). Studies demonstrate α-fodrin to regulate exocytosis via its interaction with t-SNARE syntaxin family of proteins (Nakano et al., 2001). The c-terminal coiled coil region of syntaxin interacts with α-fodrin, a major component of the submembranous cytoskeleton. Similarly, vimentin filaments interact with SNAP23/25 and hence are able to control the availability of free SNAP23/25 for assembly of the SNARE complex (Faigle et al., 2000). All these findings suggest that vimentin, α-fodrin, actin, and SNAREs may all be part of the fusion pore complex. Additional proteins such as v-SNARE (VAMP or synaptobrevin), synaptophysin and myosin, may associate when the fusion pore establishes continuity with the secretory vesicle membrane. The globular tail domain of myosin V contains binding site for VAMP which is bound in a calcium independent manner (Ohyama et al., 2001). Further interaction of myosin V with syntaxin requires both calcium and calmodulin. It has been suggested that VAMP acts as a myosin V receptor on secretory vesicles and regulates formation of the SNARE complex (Ohyama et al., 2001). Interaction of VAMP with synaptophysin and myosin V was also observed by Prekereis and Terrian (1997). To understand the fusion pore in greater detail, the composition of the fusion pore was examined using SNAP-23 specific immunoprecipitation studies on total pancreatic homogenates. In agreement with earlier findings in other tissues (Bennett, 1990; Cho et al., 2002c; Faigle et al., 2000; Goodson et al., 1997; Nakano et al., 2001; Ohyama et al., 2001; Rothman, 1994; Weber et al., 1998), our study demonstrated the association of SNAP-23 with syntaxin 2, with cytoskeletal proteins, actin, α-fodrin, and vimentin, and calcium channels β3 and α1c, together with the SNARE regulatory protein, NSF (Jena et al., 2003). These earlier studies demonstrate that the fusion pore is a cup-shaped lipoprotein basket at the cell PM where secretory vesicles dock and fuse to release vesicular contents. The base of the fusion pore complex is where t- and v-SNAREs interact in a circular array to form a conducting pore, and hence the structure was named the ''porosome''. In the present study, we have isolated the porosome, reconstituted its structure and function in artificial lipid membrane, and further characterized its morphology and biochemical composition.

MATERIALS AND METHODS

Isolation of pancreatic acini and plasma membrane preparation

Pancreatic acini were isolated for atomic force microscopy and transmission electron microscopy using minor modification of published procedure (Jena et al., 1991,2003). Male Sprague Dawley rats weighing 80–120 g were euthanized using CO_2 inhalation. Pancreas was dissected and diced into 0.5-mm^3 using a razor blade, and mildly agitated for 10 min at 37°C in a siliconized glass tube with 5 ml of oxygenated buffer A (98 mM NaCl, 4.8 mM KCl, 2 mM $CaCl_2$, 1.2 mM $MgCl_2$, 0.1% bovine serum albumin, 0.01% soybean trypsin inhibitor, 25 mM Hepes, pH 7.4) containing 1,000 units of collagenase. The acinar suspension was filtered through a 224-μm SpectraMesh (Spectrum Laboratory Products, Rancho Dominguez, CA) polyethylene filter to remove large clumps of acini and undissociated tissue. The acini were then washed six times, in ice-cold buffer A, using 50 ml per wash. Isolated rat pancreatic acini and acinar cells were plated on Cell-Tak-coated (Collaborative Biomedical Products, Bedford, MA) glass coverslips or mica for 2–3 h, before imaging using the AFM. Pancreatic PM fractions were isolated using a modification of a published method (Rosenzweig et al., 1983). After isolation and dicing of the pancreas into 0.5 mm^3 pieces using a razor blade, the diced tissue was homogenized in 15% (wt/vol) ice-cold homogenization buffer (1.25 M sucrose, 0.01% trypsin inhibitor, and 25 mM Hepes, pH 6.5). Four strokes, at maximum speed, of a motor-driven pestle (Wheaton overhead stirrer) was used to homogenize the tissue. One-and-a-half milliliter of the homogenate was layered over a 125-μl cushion of 2 M sucrose and 500 μl of 0.3 M sucrose was layered onto the homogenate in Beckman centrifuge tubes. After centrifugation at 145,000 $\times$ g for 90 min in a Sorvall AH-650 rotor, the plasma membrane (PM) banding between the 1.2 M and 0.3 M sucrose interface was collected and its protein concentration determined using the Bradford assay (Bradford, 1976). Fresh PM was prepared and used in all AFM studies.

Atomic force microscopy

Live pancreatic acinar cells and isolated PM, and immunoisolated fusion pores in PBS pH 7.5, were imaged using the AFM (Bioscope III, Digital Instruments, Woodbury, NY) in both contact and tapping modes. All AFM micrographs in this manuscript were obtained in the ''tapping'' mode in fluid, using silicon nitride tips with a spring constant of 0.06 $N \bullet m^{-1}$, and an imaging force of <200 pN. Images were obtained at line frequencies of 1 Hz, with 512 lines per image, and constant image gains. Topographical dimensions were analyzed using the software nanoscopeIIIa4.43r8 supplied by Digital Instruments.

Isolation of zymogen granules

ZGs were isolated by using a modification of the method of Jena et al. (1991). Male Sprague-Dawley rats weighing 80–120 g were euthanized using CO_2 inhalation. For every ZG preparation, the pancreas was dissected and diced into 0.5-mm^3 pieces. The diced pancreas was suspended in 15% (wt/vol) ice-cold homogenization buffer (0.3 M sucrose, 25 mM Hepes, pH 6.5, 1 mM benzamidine, 0.01% soybean trypsin inhibitor) and homogenized using three strokes of a Teflon glass homogenizer. The resultant homogenate was centrifuged for 5 min at 300 $\times$ g and a temperature of 4°C to obtain a supernatant fraction. Each volume of the supernatant fraction was mixed with 2 vol of a Percoll-Sucrose-Hepes buffer (0.3 M sucrose, 25 mM Hepes, pH 6.5, 86% Percoll, 0.01% soybean trypsin inhibitor) and centrifuged for 30 min at 16,400 $\times$ g at 4°C. Pure ZGs were obtained as a loose white pellet at the bottom of the centrifuge tube, and processed for electron microscopy.

Immunoisolation of the fusion pore and immunoblot analysis

Fusion pores were immunoisolated from PM preparations, using a SNAP-23 specific antibody. Protein in all fractions was estimated using the Bradford assay (Bradford, 1976). To isolate the fusion complex for immunoblot analysis and reconstitution experiments, SNAP-23 specific antibody conjugated to protein A-sepharose was used. Isolated pancreatic plasma membrane preparations were solubilized in Triton/Lubrol solubilization buffer (0.5% Lubrol; 1 mM benzamidine; 5 mM ATP; 5 mM EDTA; 0.5% Triton X-100, in PBS), supplemented with protease inhibitor mix (Sigma, St. Louis, MO). SNAP-23 antibody conjugated to the protein A-sepharose was incubated with the solubilized membrane for 1 h at room temperature

followed by washing with wash buffer (500 mM NaCl, 10 mM TRIS, 2 mM EDTA, pH = 7.5). The immunoprecipitated sample attached to the immunosepharose beads was incubated in Laemmli sample preparation buffer (Laemmli, 1970), before the one-dimensional (1D) 12.5% SDS-PAGE, electrotransfer to nitrocellulose, and immunoblot analysis using specific antibodies to actin (Sigma), fodrin (Santa Cruz Biotechnology Inc., Santa Cruz, CA), vimentin (Sigma), syntaxin 2 (Alomone Labs, Jerusalem, Israel), and Ca^{2+}-α1c (Alomone Labs). Similarly, for the two-dimensional (2D) gel electrophoresis, the immunoprecipitated pore complex was resolved by the published 2D 16-benzyldimethyl-*N*-hexadecylammonium chloride method (Macfarlane, 1989), followed by 1D 12.5% SDS-PAGE, electrotransferred to nitrocellulose membrane, and probed with the various antibodies. The nitrocellulose was incubated for 1 h at room temperature in blocking buffer (5% nonfat milk in PBS containing 0.1% Triton X-100 and 0.02% NaN_3), and immunoblotted for 2 h at room temperature with the specific antibody. The primary antibodies were used at a dilution of 1:5,000 in blocking buffer. The immunoblotted nitrocellulose sheets were washed in PBS containing 0.1% Triton X-100 and 0.02% NaN_3 and were incubated for 1 h at room temperature in horseradish peroxidase-conjugated secondary antibody at a dilution of 1:2,000 in blocking buffer. The immunoblots were then washed in the PBS buffer, processed for enhanced chemiluminescence and photographed using a Kodak Image Station 414.

Reconstitution of immunoisolated fusion pores into liposomes for electron microscopy studies

Large unilamellar lipid vesicles (LUV) were prepared using brain dioleoylphosphatidyl-choline (DOPC), and dioleylphosphatidylserine (DOPS), obtained from Avanti Lipids (Alabaster, AL). A 5-mM suspension of DOPC:DOPS in a ratio of 7:3, was prepared. The lipid suspension was then dried in nitrogen atmosphere, and resuspended in solution containing 10 mM HEPES pH 7.5, 140 mM NaCl, and I mM EDTA. LUVs were generated by 2–3 min of mild sonication. Immunoisolated fusion pore complexes or porosomes were reconstituted into lipid vesicles using gentle agitation for 30 min at room temperature. The reconstituted liposomes were fixed and processed for TEM.

Transmission electron microscopy

Isolated rat pancreatic acini, ZGs, and liposome-reconstituted fusion pores, were fixed in 2.5% buffered paraformaldehyde for 30 min, and the pellets were embedded in Unicryl resin and were sectioned at 40–70 nm. Thin sections were transferred to coated specimen TEM grids, dried in the presence of uranyl acetate and methyl cellulose, and examined using a transmission electron microscope. For negative staining electron microscopy, purified protein suspensions in PBS, were adsorbed onto hydrophilic carbon support films that were mounted onto formvar-coated, metal specimen grids (EMS, Ft. Washington, PA). The adsorbed protein was washed in double-distilled water and negatively stained using 1% aqueous uranyl acetate. After the grids were dried in the presence of the uranyl acetate solution, they were examined by transmission electron microscopy. To prevent bleaching by the electron beam, micrographs were obtained on portions of the grid not previously examined.

Reconstituted fusion pore into lipid bilayer for electrophysiological measurements

Lipid bilayers were prepared using brain phosphatidylethanolamine (PE) and phosphatidylcholine (PC), and dioleoylphosphatidylcholine (DOPC), and dioleylphosphatidyl-serine (DOPS), obtained from Avanti Lipids (Alabaster, AL). A suspension of PE:PC in a ratio of 7:3, and at a concentration of 10 mg/ml was prepared. Lipid suspension (100 μl) was dried under nitrogen gas and resuspended in 50 μl of decane. To prepare membranes reconstituted with the immunoisolated fusion pore complex, the immunoisolate was added to the lipid suspension and brushed onto a 200-μm hole in the bilayer preparation cup until a stable bilayer with a capacitance between 100 and 250 pF was established. Alternately, the immunoisolated pore complex was brushed onto a stable membrane formed at the 200-μm hole in the bilayer preparation cup. Electrical measurements of the artificial lipid membrane were performed using a bilayer setup (Cho et al., 2002e). Current versus time traces were recorded using pulse software, an EPC9 amplifier and probe from HEKA (Lambrecht, Germany). Briefly, membranes were formed while holding at 0 mV. Once a bilayer was formed and demonstrated to be in the capacitance limits for a stable bilayer membrane according to the hole diameter, the voltage was switched to −60 mV. A baseline current was established before the addition of ZG.

RESULTS AND DISCUSSION

Details of the native fusion pore revealed from AFM and TEM Studies

As reported earlier (Cho et al., 2002c; Schneider et al., 1997), pancreatic acinar cells in physiological buffer reveal the presence of ''pits'' measuring 0.4–1 μm in diameter, which contain ''depressions'' or fusion pores. Each fusion pore measures ~125–185 nm in diameter and 19–25 nm in relative depth (Fig. 2, *a* and *c*). AFM micrographs demonstrate the localization of gold-labeled antiamylase at the opening of fusion pores after stimulation of secretion demonstrating the release of ZG contents through the pores (Cho et al., 2002c). To determine the morphology of the fusion pore at the cytosolic side, a pancreatic PM preparation was used. Isolated PM in buffer when placed on freshly cleaved mica, tightly adheres to the mica surface, allowing high resolution AFM imaging. The PM preparations contain scattered circular disks measuring 0.5–1 μm in diameter, with inverted cup-shaped structures within (Fig. 2, *b* and *d*). The inverted cups range in height from 20–25 nm. On several occasions, ZGs, 0.4–0.8 μm in diameter, are found associated with one or more of the inverted cups (Cho et al., 2002c) suggesting them to be the base of the fusion pores. To conclusively determine whether the cup-shaped structures in isolated PM preparations are indeed the fusion pores, immunoAFM studies were performed. The t-SNARE protein, SNAP-23, has been identified and implicated in secretion from pancreatic acinar cells (Gaisano et al., 1997). A polyclonal monospecific SNAP-23 antibody, recognizing a single 23 kDa band in an immunoblot analysis of a pancreatic homogenate, was used in immunoAFM studies. When the SNAP-23 specific antibody was added to the PM preparation during imaging using the AFM, the antibody specifically localized to the base of the cup-shaped structure that represents the tip of the inverted cup (Cho et al., 2002c). No antibody labeling of the structure was detected when preimmune serum was applied. These results demonstrated that the inverted cup-shaped structures in isolated PM preparations are the fusion pores observed from its cytosolic side. To further confirm our AFM studies, and to have a better understanding of the fusion pore, transmission electron microscopy was performed.

Fusion pores are relatively small structures (125–185 nm in diameter at its wide end, and 10–40 nm at the base), and are present only at the apical plasma membrane (PM) of pancreatic acinar cells, hence it is extremely difficult and rare to be able to obtain a cross section through the structure along with any associated secretory vesicles. Nonetheless, such structures can be observed in electron micrographs of isolated cells and tissue preparations (Figs. 3 and 4; Jena et al., 2003). In Fig. 3, the electron micrograph of a fusion pore sectioned at a certain angle, depicts its distinct and separate bilayer, and the bilayer attachment of the associated secretory vesicle, the zymogen granule (ZG). A cross section through three lateral knob-like structures that circle around the fusion pore basket, are clearly delineated. The apical knob-like structure at the lip of the pore appear the largest. The TEM micrograph further demonstrates that the lower knobs are the site for attachment of the ZG membrane.

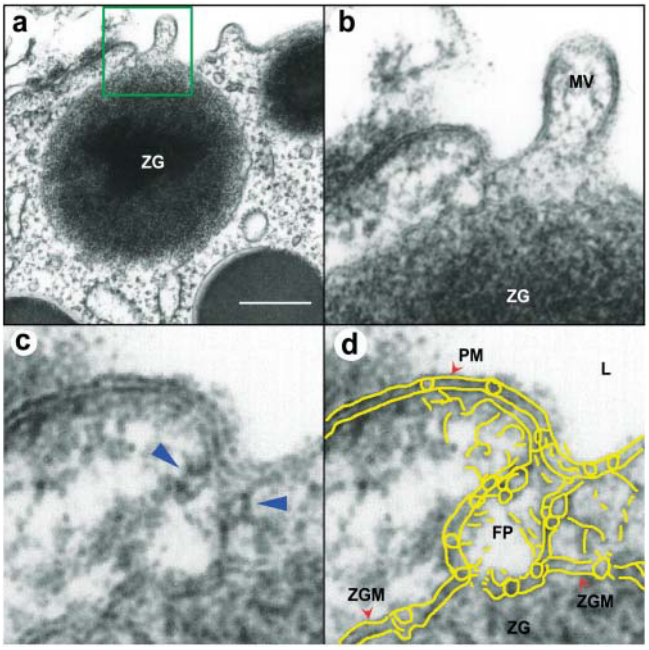

FIGURE 3 Transmission electron micrograph of a porosome associated with a docked secretory vesicle at the apical end of a pancreatic acinar cell. (*a*) Part of the apical end of a pancreatic acinar cell demonstrating within the green bordered square, the presence of a fusion pore or porosome and an associated zymogen granule (*ZG*), the electron dense secretory vesicle of the exocrine pancreas. (Bar = 400 nm; Fig 2 *a* only). The area within the green square in *a* has been enlarged to show the apical microvilli (*MV*) and a section through porosome and the ZG. Note the ZG membrane (*ZGM*) bilayer is attached directly to the base of the porosome cup. A higher magnification of the porosome in *c* depicts in further detail the porosome bilayer and cross section through the three protein rings, with the thicker ring (*blue arrowhead*) present close to the opening of the porosome to the outside. The third and the lowest ring away from the porosome opening is attached to the ZGM. (*d*) Yellow outline of the fusion pore (*FP*) or the porosome membrane shows the continuity with the apical plasma membrane (*PM*) at the apical end of the pancreatic acinar cell facing the lumen (*L*), and also defines the exact points of contact of the ZGM with the porosome membrane.

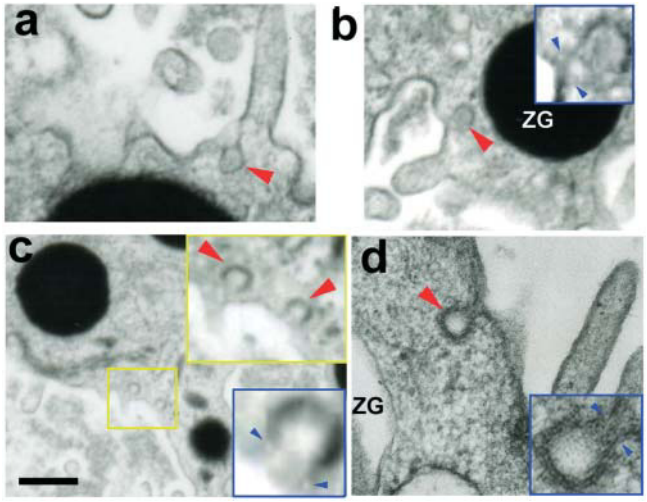

FIGURE 4 Transmission electron micrographs of porosomes (*red arrowheads*) at the apical end of pancreatic acinar cells. Note the thicker ring (*blue arrowhead*) present close to the opening of each porosome, shown in the enlarged images of the porosomes within insets having blue margins. Bar = 200 nm (not applicable to *insets*).

Although not so detailed, similar porosome or fusion pore structures are also depicted in the electron micrographs in Fig. 4. TEM studies confirm the fusion pore to have a cup-shaped structure, with similar dimensions as determined in all our earlier AFM and electron microscopy (EM) studies (Cho et al., 2002a,b,c,d; Schneider et al., 1997; Jena et al., 2003). Additionally, TEM results reveal that the fusion pore, has a basket-like morphology, with three lateral and a number of vertically arranged ridges. A ring-like structure is also observed at the base of the fusion pore cup. Because these PM structures are stable, we hypothesized that, if membrane-bounded ZGs were to fuse at the base of the fusion pore, they would co-isolate with ZGs. To test this hypothesis, ZGs were isolated and the preparation was processed for TEM. Our TEM studies confirmed this hypothesis and revealed the isolation of the fusion pore associated with docked vesicle (Fig. 5; Jena et al., 2003). As was observed in TEM of whole acinar cells (Figs. 3 and 4), the PM and ZG membrane are clearly distinct in the isolated fusion pore-ZG preparations (Fig. 5). The apical knob-like structure at the lip of the pore is also evident in the isolated fusion pore-ZG preparations. The fusion pores reveal both lateral and vertical structures originate from within the complex (Fig. 5). These vertical structures appear attached to the fusion pore membrane. The presence of such vertical ridges lining the fusion pore in NG108-15 nerve cells have been previously reported (Tojima, et al., 2000). In our TEM micrographs, both in the whole cell and in the ZG-associated complex, the lateral ridges are clearly defined, with a prominent lip ridge at the pore opening. Vertical ridges are evident in electron micrographs of fusion pores associated with isolated ZGs. Thus, the combination of AFM and TEM studies have

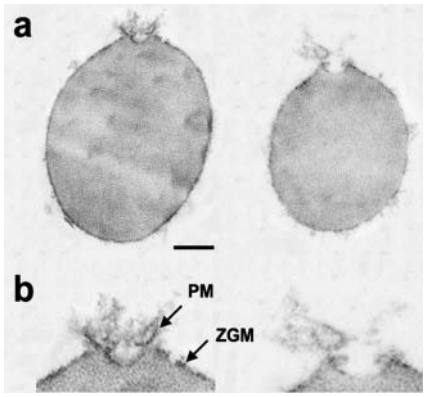

FIGURE 5 Transmission electron micrographs of zymogen granules (ZGs), co-isolated with fusion pores or porosomes. (*a*) Fusion pores associated at the surface of ZGs are shown. (Bar = 120 nm; *top panel* only). (*b*) At higher magnification details of the fusion pore, demonstrating the presence of separate plasma membrane (*PM*) and the ZG membrane (*ZGM*). Note the apically arranged ring complex of the fusion pore, similar to what is observed in electron micrographs of the fusion pore in intact cells (Fig. 2).

provided a clear understanding of the fusion pore morphology. Earlier studies reporting the association of t-SNAREs with secretory vesicles (Otto et al., 1997), could be due to the co-isolation of the fusion pore containing t-SNAREs in secretory vesicle preparations (Fig. 5; Jena et al., 2003).

Composition of the fusion pore complex

In a recent study (Cho et al., 2002e), purified SNARE proteins and artificial lipid membranes were used to demonstrate that t- and v-SNAREs, located in opposing bilayers, interact in a circular array to form conducting pores. A ring-like structure is observed at the base of the fusion pore complex, and SNAP-23 immunoreactivity has been localized to the site (Cho et al., 2002e), demonstrating the presence of t-SNAREs at the base of the fusion pore cup. To determine the association of other proteins with the fusion pore complex, immunoprecipitation studies on solubilized pancreatic PM using SNAP-23 specific antibody were performed. The precipitated sample was resolved using 12.5% SDS-PAGE, transferred to a nitrocellulose membrane, and probed using various antibodies. In agreement with earlier findings in other tissues (Bennett, 1990; Cho et al., 2002c; Faigle et al., 2000; Goodson et al., 1997; Nakano et al., 2001; Ohyama et al., 2001; Rothman, 1994; Weber et al., 1998), our study demonstrates the association of SNAP-23 with syntaxin 2, with cytoskeletal proteins, actin, α-fodrin, and vimentin, and calcium channels α1c, together with the SNARE regulatory protein, NSF (Jena, et al., 2003). Additionally, in the present study, chloride ion channels ClC2 and ClC3 were identified as part of the fusion pore complex. To determine the presence of isoforms, if any, of the various proteins identified in the SNAP-23 antibody immunoprecipitated sample, 2D gel electrophoresis (16-

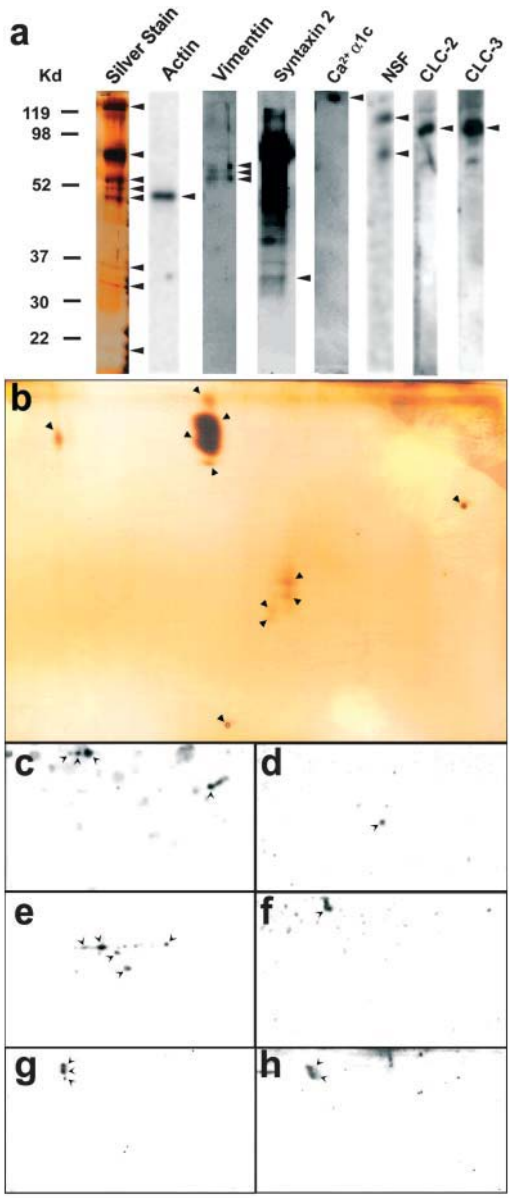

FIGURE 6 One (1D) and two dimensionally (2D) resolved proteins immunoisolated from solubilized pancreatic plasma membrane preparations, using a SNAP-23 specific antibody. The resolved proteins were silver stained and transferred to nitrocellulose membranes for immunoblot analysis. Note the identification in the immunoisolates of eight protein bands in a silver-stained SDS-PAGE 1D-resolved gel. (the *far left panel* in *a*). Immunoblot analysis of the 1D-resolved immunoisolated proteins demonstrate the presence of actin, vimentin, syntaxin-2, calcium channel, NSF, and chloride channels CLC-2 and CLC-3. (*b*) 2D resolution of the immunoisolated proteins, provide eleven spots in a silver stained gel. Immunoblot analysis of the 2D-resolved immunoisolated proteins further demonstrates the presence of isoforms of some of the proteins identified in *a*. (*c*) There appears to be at least three isoforms of the calcium channel: (*d*) one isoform of actin; (*e*) three isoforms of vimentin, (*f*) one NSF; (*g*) one each of the CLC-2; and (*h*) the CLC-3. Arrows pointing to lower molecular weights may represent proteolytic cleavage products.

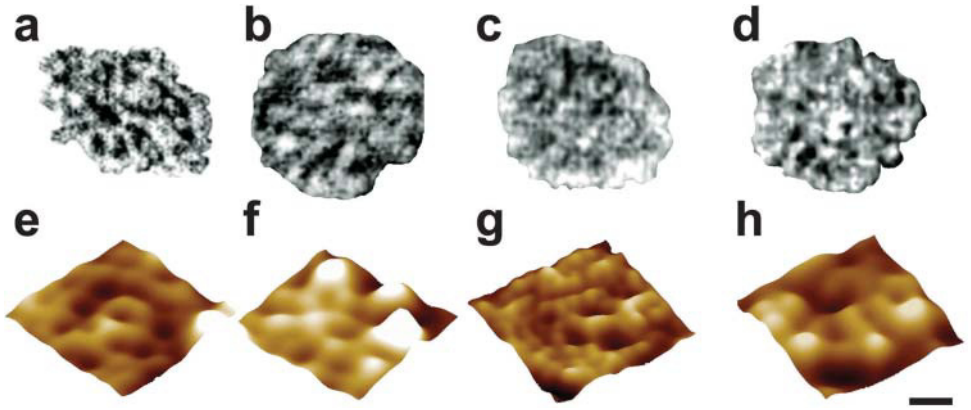

FIGURE 7 Four separate sets of negatively stained electron micrographs and four sets of atomic force micrographs of the immunoisolated fusion pore or porosome complex. Note the similarity in size and morphology of the complex. Bar = 30 nm.

BAC followed by SDS-PAGE gels) was performed to further resolve the immunoprecipitates. Three isoforms each of the calcium ion channel and vimentin were clearly identifiable (Fig. 6). Although multiple spots are identified in several of the immunoblots, the low molecular weight spots may represent proteolytic degredation of the parent molecule. To determine the number of major proteins immunoisolated, both the 1D and 2D gels were silver stained. A total of eight major bands were detectable using 1D and 11 spots by 2D gels. The immunoblots, however, demonstrate the presence of other proteins in the immunoisolate, undetectable by silver stain. Sequence analysis of the major spots identified by silver stain in the 2D gel, will further help in their identification. Next it was important to determine the morphology and size of this immunoisolated supramolecular complex. This structural analysis was performed by both AFM and TEM.

Morphology of the immunoisolated supramolecular porosome complex

The size and shape of the immunoisolated supramolecular porosome complex was examined using both negative staining electron microscopy on the dehydrated sample, and on the hydrated sample in near physiological buffer using the AFM (Figs. 7 and 8). EM and AFM images of the immunoisolated porosome complex were found to be similar, if not identical. Although some images are better then others, all images exhibit similar morphology. Because these are not 2D crystals of isolated fusion pore complexes in lipid membranes, they may settle differently on the substrate (carbon-coated grid for EM and mica or glass for AFM imaging). Sometimes, the complex may fold by different degrees. Hence, complexes that lie flat and evenly on the substrate, provide more detailed morphology of the protein skeleton of the fusion pore complex (such as the one shown

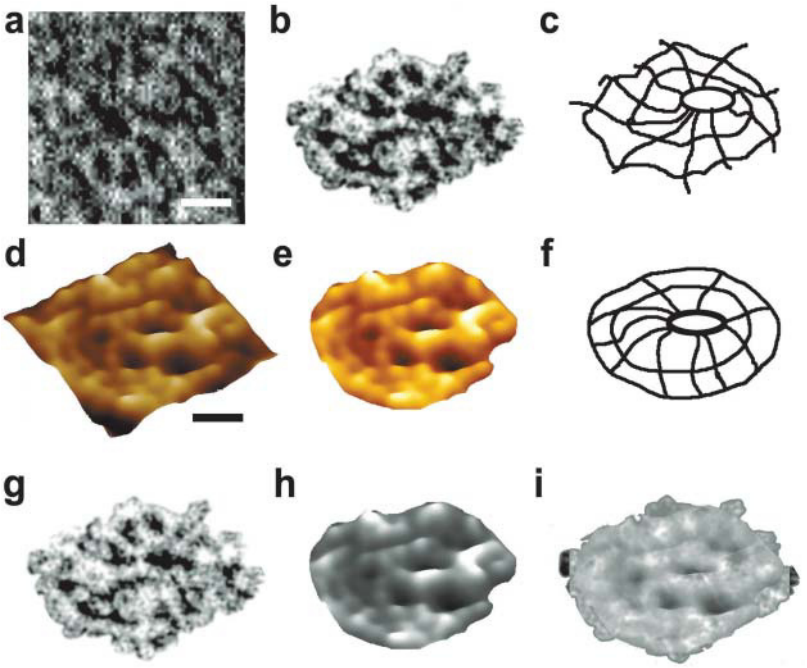

FIGURE 8 Negatively stained electron micrograph and atomic force micrograph of the immunoisolated fusion pore complex. (*a*) Negatively stained electron micrograph of an immunoisolated fusion pore complex from solubilized pancreatic plasma membrane preparations, using a SNAP-23 specific antibody. Note the three rings and the 10 spokes that originate from the inner smallest ring. This structure represents the protein backbone of the fusion pore complex, because the three rings and the vertical spikes are observed in electron micrographs of cells and fusion pores co-isolated with ZGs. Bar = 30 nm. (*b*) The electron micrograph of the fusion pore complex, cut out from *a*, and (*c*) an outline of the structure presented for clarity. (*d–f*) Atomic force micrograph of the isolated pore complex in near physiological buffer. Bar = 30 nm. Note the structural similarity of the complex, imaged both by TEM (*g*) and AFM (*h*). The TEM and AFM micrographs are superimposable (*i*).

in Figs. 7, *a* and *g*, and 8). Such clear images of the immunoisolated porosome complex, obtained using both EM (Fig. 8, *a–c*) and AFM (Fig. 8, *d–f*), demonstrate the supramolecular complex to be almost identical and interestingly almost superimposable (Fig. 8 *i*). The pure supramolecular complex is found to be a 125–150-nm oval-shaped structure with three concentric rings and ~10 spokes that originate from the small inner ring and traverse the larger two outer rings. The supramolecular complex has close similarity to the electron micrograph of the membrane-associated fusion pore complex (Fig. 3–5). The central ring has a diameter of ~25–30 nm, with a 20–25-nm central opening, similar to the pore formed when t-SNAREs and v-SNARE in opposing bilayers meet (Cho et al., 2002e). Hence, the supramolecular complex appeared to be the fusion pore complex or porosome (Jena et al., 2003), without its lipid bilayer. To test this hypothesis, the immunoisolated supramolecular complex was reconstituted into artificial liposomes, and the liposome-reconstituted complex examined using TEM (Fig. 9). Transmission electron micrographs reveal a 150–200-nm cup-shaped basket-like structure (Fig. 9) as observed of the fusion pore when co-isolated with ZGs (Fig. 5), in ZG preparations. The important question then remained: are such reconstituted porosomes functional? To answer this question, the complex was reconstituted into a lipid bilayer membrane in an electrophysiological-membrane setup that could monitor changes in the reconstituted membrane under various experimental conditions.

Reconstituted fusion pore is a functional supramolecular complex

When the supramolecular porosome complex was reconstituted into a lipid bilayer membrane in an electrophysio-

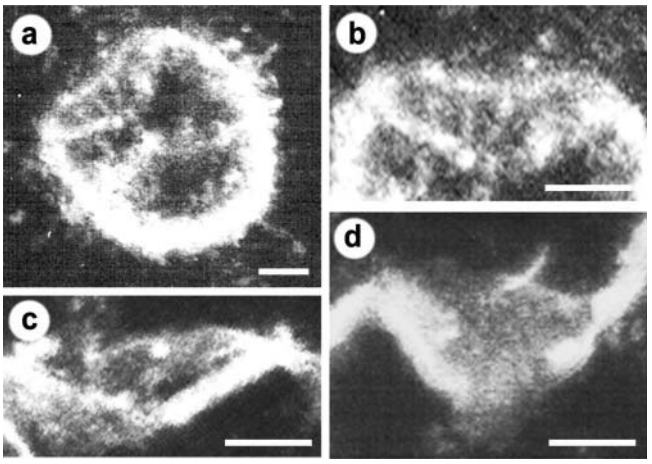

FIGURE 9 Electron micrographs of reconstituted porosome or fusion pore complex in liposomes. showing a cup-shaped basket-like morphology. (*a*) A 500-nm vesicle with an incorporated porosome is shown. Note the spokes in the complex. The reconstituted complex at greater magnification is shown in *b–d*. Bar = 100 nm.

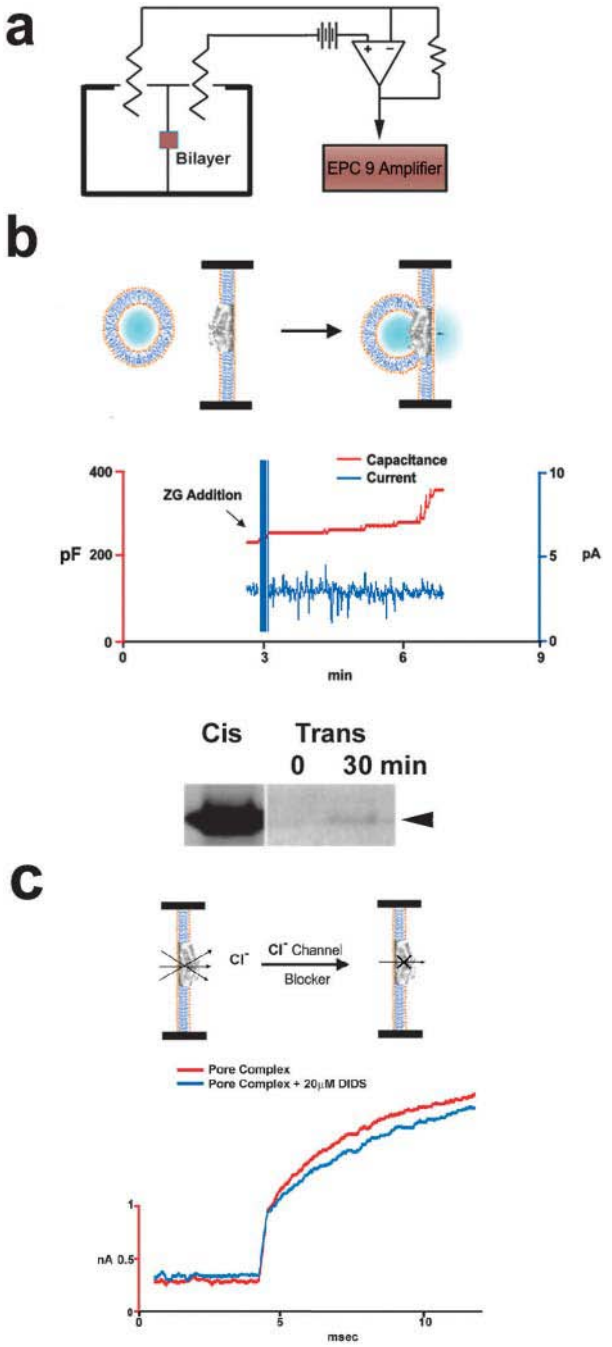

FIGURE 10 Lipid bilayer-reconstituted porosome complex is functional. (*a*) Schematic drawing of the bilayer setup for electrophysiological measurements. (*b*) Zymogen granules (ZGs) added to the *cis* side of the bilayer fuse with the reconstituted porosomes, as demonstrated by an increase in capacitance and current activities, and a concomitant time dependent release of amylase (a major ZG content) to the *trans* side of the membrane. The movement of amylase from the *cis* to the *trans* side of the chamber was determined by immunoblot analysis of the contents in the *cis* and the *trans* chamber over time. (*c*) As demonstrated by immunoblot analysis of the immunoisolated complex, electrical measurements in the presence and absence of chloride ion channel blocker DIDS, demonstrate the presence of chloride channels in association with the complex.

logical setup (Fig. 10 *a*), and ZG added to the *cis* chamber, ZG fused with the bilayer as demonstrated by an increase in capacitance and conductance, and a time-dependent release of amylase (one of the major contents of ZG) to the *trans* compartment of the EPC9 electrophysiological bilayer setup was observed. Amylase was detected by immunoblot assays (Fig. 10 *b*), using a previously characterized amylase specific antibody (Cho et al., 2002c). As seen in immunoblot assays (Fig. 6), chloride channel activity was demonstrated with the supramolecular porosome complex (Fig. 10 *c*). Further, the chloride channel inhibitor DIDS, was found to inhibit current activity in the porosome-reconstituted bilayer. Contrarily, although our immunoblot assays demonstrate the association of calcium channels with the porosome complex, we were unable to detect calcium channel activities in the reconstituted membrane. This may be due to inactivation of the associated calcium channel in the complex as a result of the immunoisolation procedures used in our study. The role of the chloride channel in the fusion pore is unknown at this time. These studies demonstrate that the fusion pore or porosome is a 125–150-nm macromolecular cup-shaped lipoprotein basket at the cell PM, where membrane-bound secretory vesicles dock and fuse to release vesicular contents. ImmunoTEM combined with immunoAFM will further help determine the specific arrangement and localization of the various porosome-associated proteins.

This work was supported in part by the National Institutes of Health (research grants DK56212 and NS39918 to B.P.J.). S.-J.C. is a recipient of a National Institutes of Health postdoctoral fellowship award (DK60368).

REFERENCES

Bennett, V. 1990. Spectrin-based membrane skeleton: a multipotential adaptor between plasma membrane and cytoplasm. *Physiol. Rev.* 70: 1029–1065.

Bradford, M. M. 1976. A rapid and sensitive method for the quantitation of microgram quantities of protein utilizing the principle of protein-dye binding. *Anal. Biochem.* 72:248–254.

Cho, S.-J., K. Jeftinija, A. Glavaski, S. Jeftinija, B. P. Jena, and L. L. Anderson. 2002a. Structure and dynamics of the fusion pores in live GH-secreting cells revealed using atomic force microscopy. *Endocrinology.* 143:1144–1148.

Cho, S.-J., A. Wakade, G. D. Pappas, and B. P. Jena. 2002b. New structure involved in transient membrane fusion and exocytosis. *Ann. New York Acad. Sci.* 971:254–256.

Cho, S.-J., A. S. Quinn, M. H. Stromer, S. Dash, J. Cho, D. J. Taatjes, and B. P. Jena. 2002c. Structure and dynamics of the fusion pore in live cells. *Cell Biol. Int.* 26:35–42.

Cho, S.-J., J. Cho, and B. P. Jena. 2002d. The number of secretory vesicles remains unchanged following exocytosis. *Cell Biol. Int.* 26:29–33.

Cho, S.-J., M. Kelly, K. T. Rognlien, J. Cho, J. K. H. Hoerber, and B. P. Jena. 2002e. SNAREs in opposing bilayers interact in a circular array to form conducting pores. *Biophys. J.* 83:2522–2527.

Faigle, W., E. Colucci-Guyon, D. Louvard, S. Amigorena, and T. Galli. 2000. Vimentin filaments in fibroblasts are a reservoir for SNAP-23, a component of the membrane fusion machinery. *Mol. Biol. Cell.* 11:3485–3494.

Gaisano, H. Y., L. Sheu, P. P. Wong, A. Klip, and W. S. Trimble. 1997. SNAP-23 is located in the basolateral plasma membrane of rat pancreatic acinar cells. *FEBS Lett.* 414:298–302.

Goodson, H. V., C. Valetti, and T. E. Kreis. 1997. Motors and membrane traffic. *Curr. Opin. Cell Biol.* 9:18–28.

Jena, B. P., P. J. Padfield, T. S. Ingebritsen, and J. D. Jamieson. 1991. Protein tyrosine phosphatase stimulates Ca(2+)-dependent amylase secretion from pancreatic acini. *J. Biol. Chem.* 266:17744–17746.

Jena, B. P., S.-J. Cho, A. Jeremic, M. H. Stromer, and R. Abu-Hamdah. 2003. Structure and composition of the fusion pore. *Biophys. J.* 84:1337–1343.

Laemmli, U. K. 1970. Cleavage of structural proteins during the assembly of the head of bacteriophage T4. *Nature.* 227:680–685.

Macfarlane, D. E. 1989. Two dimensional benzyldimethyl-n-hexadecylammonium chloride sodium dodecyl sulfate preparative polyacrylamide gel electrophoresis: a high capacity high resolution technique for the purification of proteins from complex mixtures. *Anal. Biochem.* 176:457–463.

Nakano, M., S. Nogami, S. Sato, A. Terano, and H. Shirataki. 2001. Interaction of syntaxin with α-fodrin, a major component of the submembranous cytoskeleton. *Biochem. Biophys. Res. Commun.* 288:468–475.

Ohyama, A., Y. Komiya, and M. Igarashi. 2001. Globular tail of myosin-V is bound to vamp/synaptobrevin. *Biochem. Biophys. Res. Commun.* 280:988–991.

Otto, H., P. I. Hanson, and R. Jahn. 1997. Assembly and disassembly of a ternary complex of synaptobrevin, syntaxin, and SNAP-25 in the membrane of synaptic vesicles. *Proc. Natl. Acad. Sci. USA.* 94:6197–6201.

Prekereis, R., and D. M. Terrian. 1997. Brain myosin V is a synaptic vesicle-associated motor protein: evidence for a Ca^{2+}-dependent interaction with the synaptobrevin-synaptophysin complex. *J. Cell Biol.* 137:1589–1601.

Rosenzweig, S. A., L. J. Miller, and J. D. Jamieson. 1983. Identification and localization of cholecystokinin-binding sites on rat pancreatic plasma membranes and acinar cells: a biochemical and autoradiographic study. *J. Cell Biol.* 96:1288–1297.

Rothman, J. E. 1994. Mechanism of intracellular protein transport. *Nature.* 372:55–63.

Schneider, S. W., K. C. Sritharan, J. P. Geibel, H. Oberleithner, and B. P. Jena. 1997. Surface dynamics in living acinar cells imaged by atomic force microscopy: identification of plasma membrane structures involved in exocytosis. *Proc. Natl. Acad. Sci. USA.* 94:316–321.

Tojima, T., Y. Yamane, H. Takagi, T. Takeshita, T. Sugiyama, H. Haga, K. Kawabata, T. Ushiki, K. Abe, T. Yoshioka, and E. Ito. 2000. Three-dimensional characterization of interior structures of exocytotic apertures of nerve cells using atomic force microscopy. *Neuroscience.* 101:471–481.

Weber, T., B. V. Zemelman, J. A. McNew, B. Westerman, M. Gmachl, F. Parlati, T. H. Söllner, and J. E. Rothman. 1998. SNAREpins: minimal machinery for membrane fusion. *Cell.* 92:759–772.